

Resistance Spot Welded AZ31 Magnesium Alloys, Part II: Effects of Welding Current on Microstructure and Mechanical Properties

L. LIU, L. XIAO, J.C. FENG, Y.H. TIAN, S.Q. ZHOU, and Y. ZHOU

Resistance spot welding of AZ31 magnesium alloys from different suppliers, AZ31-SA (from supplier A) and AZ31-SB (from supplier B), was studied and compared in this article. The mechanical properties and microstructures have been studied of welds made with a range of welding currents. For both groups of welds, the tension-shear fracture load (F_C) and fracture toughness (K_C) increased with the increase in welding current. The F_C and K_C of AZ31-SA welds were larger than those of AZ31-SB welds. The fracture surfaces of AZ31-SB welds were relatively flatter than those of AZ31-SA. Microstructural examination via optical microscope demonstrated that almost all weld nuggets comprised two different zones, the columnar dendritic zone (CDZ), which grew epitaxially from the fusion boundary, and the equiaxed dendritic zone (EDZ), which formed in the center of the nugget. The nature and extent of the CDZ seemed to be critical to the strength and toughness of spot welds because of its position adjacent to the inherent external circular crack-like notch of spot welds and the stress concentration in this region. The width and microstructure of the CDZ were different between AZ31-SA and AZ31-SB. The AZ31-SA alloy produced finer and shorter columnar dendrites, whereas the AZ31-SB alloy produced coarser and wider columnar dendrites. The width of the CDZ close to the notch decreased with the increase of current. The CDZ disappeared when the current was higher than a critical value, which was about 24 kA for AZ31-SA and 28 kA for AZ31-SB. The microhardness of the two base materials was the same, but within the CDZ and EDZ, the hardness was greater in AZ31-SA than AZ31-SB welds. It is believed that the different microstructures of spot welds between AZ31-SA and AZ31-SB resulted in different mechanical properties; in particular, K_C increased with the welding current because of the improved columnar-to-equiaxed transition.

DOI: 10.1007/s11661-010-0339-7

© The Minerals, Metals & Materials Society and ASM International 2010

I. INTRODUCTION

BECAUSE of the strong demand for weight reduction and for better fuel efficiency of transportation vehicles, magnesium alloys currently are receiving strong research interest for applications to various structural components of automobiles and aircraft.^[1] Several joining processes, including gas tungsten arc, electron beam,^[2] laser,^[3] friction stir welding,^[4] and resistance spot welding^[5] (RSW), are employed and studied for the welding of Mg alloys. RSW is a primary

joining method in the auto industry because of its ability to assemble sheet metal structures efficiently. However, few feasibility studies have been published for RSW application to Mg alloys, and detailed investigations on the relationship between processing, mechanical properties, and microstructure are needed.^[5-7] Generally, the microstructure of Mg spot welds includes both columnar dendritic and equiaxed dendritic structures.^[7] It is accepted widely that changing the morphology of the solidification structure in the weld (fusion zone) from coarse columnar to fine equiaxed grains can improve the mechanical properties of the weld.^[8,9]

Columnar-to-equiaxed transition (CET) during nugget solidification has been proposed to be caused either by a pileup of equiaxed crystals that block the growth of the columnar grains or by attachment of equiaxed crystals from the liquid to the columnar dendrite front.^[10,11] The criteria for CET are tip growth rate and temperature gradients ahead of the dendrite tips.^[9,12] Various techniques have been employed to promote CET and increase the percentage of equiaxed grains in the weld, such as magnetic arc oscillation,^[13] ultrasonic vibration,^[14] exciting the electric arc,^[15] or double-sided arc welding.^[16] However, changing the welding parameters^[9] and the addition of heterogeneous

L. LIU, Ph.D. Candidate, is with the State Key Laboratory of Advanced Welding Production Technology, Harbin Institute of Technology, Harbin 150001, P.R. China, and with the Department of Mechanical and Mechatronics Engineering, University of Waterloo, Waterloo N2L 3G1, Canada. L. XIAO, Ph.D. Candidate, and Y. ZHOU, Professor, are with the Department of Mechanical and Mechatronics Engineering, University of Waterloo. Contact e-mail: nzhou@mecheng1.uwaterloo.ca J.C. FENG, Professor, and Y.H. TIAN, Assistant Professor, are with the State Key Laboratory of Advanced Welding Production Technology, Harbin Institute of Technology. S.Q. ZHOU, Professor, is with the School of Mechanical Science and Engineering, Huazhong University of Science and Technology, Wuhan 430074, P.R. China.

Manuscript submitted August 25, 2009.

Article published online June 25, 2010

nucleation elements^[17] are the most prevalent and straightforward methods used in industrial welding practice.

Our previous study has shown that AZ31 alloys from two suppliers, with nearly the same chemical composition and sheet thickness, produced a different fusion zone microstructure in RSW. Micron-sized Al₈Mn₅ secondary particles presented in the AZ31 alloy can promote CET.^[18] The objective of the current work is to investigate the effects of welding current on the CET of AZ31 resistance spot welds and, hence, the mechanical properties.

II. TECHNICAL BACKGROUND

It has been considered that from a fracture mechanics point of view, the sharp slit between two overlapping metal sheets joined by the nugget of a spot weld is actually an intrinsic three-dimensional crack. Therefore, stress intensity factors (K_I , K_{II} , and K_{III}) around the nugget can be calculated, and fracture toughness becomes an important factor for the strength of spot weld. In recent years, Zhang derived analytic equations for stress intensity factors and successfully converted the fatigue test data from load *vs* life into K_{eq} *vs* life.^[19,20] Besides loading force and nugget size, Zhang also introduced sheet thickness into the theoretical predictions. The equivalent stress intensity factor K_{eq} was defined as follows:

$$K_{eq} = \sqrt{K_I^2 + \alpha K_{II}^2 + \beta K_{III}^2} \quad [1]$$

For tension-shear testing, because of the symmetry conditions of the specimen, $\alpha = 1.0$ and $\beta = 0$, so K_{eq} becomes the following:

$$K_{eq} = \sqrt{K_I^2 + K_{II}^2} = 0.694 \frac{F}{d\sqrt{t}} \quad [2]$$

where F is tension-shear load, t is the sheet thickness, and d is the nugget size. When the load reaches its critical level, failure occurs (the crack starts to propagate). This critical value of the stress intensity factor could be considered fracture toughness (K_c , material parameter).^[21] So the fracture toughness can be expressed as follows:

$$K_c = 0.694 \frac{F_t}{d\sqrt{t}} \quad [3]$$

where F_t is failure load and K_c is the fracture toughness. However, the apparent (measured) fracture toughness value decreases with specimen thickness until a plateau is reached.^[22] This process has been explained and proved by the plane-stress–plane-strain transition model. It can be inferred that for two pieces of cracks with identical material properties, the measured fracture toughness of the thicker one should be either smaller or equal to the thinner one.

Generally, there are two failure modes for spot welds, interfacial failure and nugget pullout. For interfacial failure mode, normally little plastic deformation will be

sustained at fracture according to the force-displacement curve.^[21,23] In contrast, the pullout failure of a spot weld involves predominantly plastic shear or plastic collapse around the circumference of the weld nugget in the heat-affected zone (HAZ), and cracks do not initiate at the slit tip.^[23] So the nugget pullout mode cannot satisfy linear elastic deformation and the notch stress distribution of the model. The K_c value is only relevant in interfacial failure mode. It also should be cautioned that Eq. [3] is derived for sheets with the same metallurgical properties, although the assumption is not stated explicitly.

III. EXPERIMENTAL PROCEDURES

A. Materials and Microstructural Examination

The materials used in the current work were two commercial-grade hot-rolled sheets of magnesium alloys, AZ31-SA of 2.0 mm in thickness and AZ31-SB of 1.5 mm in thickness from two different manufacturers. Only a few AZ31-SA samples were machined down to 1.5 mm in thickness and then spot welded with the same welding conditions to compare with the AZ31-SB welds. The chemical compositions of AZ31-SA and AZ31-SB alloys were analyzed using an inductively coupled plasma–atom emission spectrometer and mass spectrometer. As Table I shows, all chemical constituents satisfied American Society for Testing and Materials (ASTM) standards. The compositions of the two alloys were nearly the same.

The microstructures of the as-received and welded specimens were examined by optical microscope and by a JEOL JSM-6460 scanning electron microscope (SEM, Japan Electron Optics Ltd., Tokyo, Japan) equipped with an Oxford (Oxford Instruments Micro-analysis Group High Wycombe, Bucks, UK) ultra-thin window detector energy-dispersive spectrometer. The metallurgical samples were cross sectioned through the weld center, mounted, ground, and polished. A solution of 4.2 g picric acid, 10 ml acetic acid, 70 ml ethanol, and 10 ml water was prepared as an etchant and briefly applied to the polished surface of each sample, which then was rinsed thoroughly with deionized water and ethanol. Both optical microscopy and scanning electron microscopy were used to examine the microstructural details. The microhardness profiles of the welds were measured on the cross sections using a HMV-2000 Vickers microhardness apparatus (Shimadzu Ltd., Kyoto, Japan). Testing was performed with 100 g force and a holding time of 15 seconds. The reported values of hardness are averages of five measurements, respectively.

Table I. Chemical Composition of the Two AZ31 Alloys (in Weight Percent)

Supplier	Al	Zn	Mn	Si	Zr	Ca	RE	Mg
AZ31-SA	2.92	1.09	0.3	0.01	<0.01	<0.01	0.01	Bal.
AZ31-SB	3.02	0.80	0.3	0.01	<0.01	<0.01	<0.01	Bal.

B. RSW and Mechanical Property Measurement

The configuration and dimensions of the welding specimens used throughout the present work are shown in Figure 1. The specimens were cut parallel to the rolling direction of the sheets. The surfaces of the plates were cleaned chemically using 2.5 pct (wt/vol) chromic acid before welding to remove surface oxidation and contamination. The spot welding was performed using a conventional Ac spot-welding machine (Centerline Ltd, Windsor, Canada). Electrode caps (FF25) with a sphere radius of 50.8 mm and a face diameter of 16 mm, manufactured from class Cu-Cr-Zr alloy, were used.

To compare the mechanical properties of the two AZ31 Mg alloys, welding parameters were controlled to ensure an interfacial failure mode. The formation and growth of weld nuggets can be divided into the following stages: incubation, growth, and stabilization.^[5] According to our previous research, after four to six cycles of welding current duration (60 cycles for 1 second), the welds in these Mg alloys no longer grew significantly, and the stabilization phase was entered. Therefore, eight cycles of weld time were selected to ensure the welds would reach a relatively stable nugget size. A lower current leads to an underdeveloped nugget size and nearly no penetration. A higher current would increase nugget size, changing the fracture mode from interfacial failure to nugget pullout, which is not related to the strength of the weld but to the strength of the HAZ. Thus, the current ranges were selected as 20 kA to 29 kA for AZ31-SA and 18 kA to 28 kA for AZ31-SB. The welding conditions are listed in Table II. Six welding samples were welded under each welding condition—three for tension-shear test and three for microstructural examination.

The mechanical properties of as-received base materials (BMs) parallel to the rolling direction were measured. The specimen geometry used in this study is designed according to the ASTM standard section B557M-06. Tension-shear tests of BMs were carried on an Instron universal test machine (Instron, Norwood, MA) at a constant strain rate of $10^{-4}/\text{s}$. Two spacers were used to compensate for coupon offset and prevent initial bending before applying tensile load. After

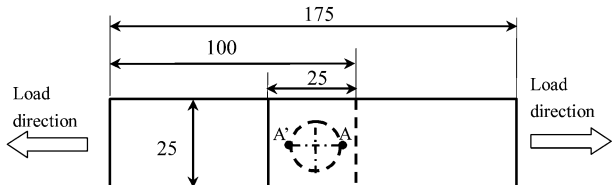


Fig. 1—Schematic diagram of RSW specimens (unit in mm).

Table II. Welding Parameters

Welding Parameter	Electrode Force kN	Welding Current kA	Welding Time Cycle	Squeezing Time Cycle	Cooling Time Cycle
AZ31-SA	4	20–29	8	30	30
AZ31-SB	4	18–28	8	30	30

fracture, fracture surfaces and metallographic specimens were analyzed using SEM. Data^[6] from our previous study on the tension-shear strength and nugget size of AZ31-SA were used in this article to compare with AZ31-SB. The test methods mentioned were the same as used in the previous study.

IV. RESULTS AND DISCUSSION

A. BMs

Typical optical microstructures of AZ31-SA and AZ31-SB alloys in the as-received condition are shown in Figures 2(a) and (b). The longitudinal (*L*) axis coincides with the plate rolling direction. The width (*W*) axis is in the specimen width direction. The

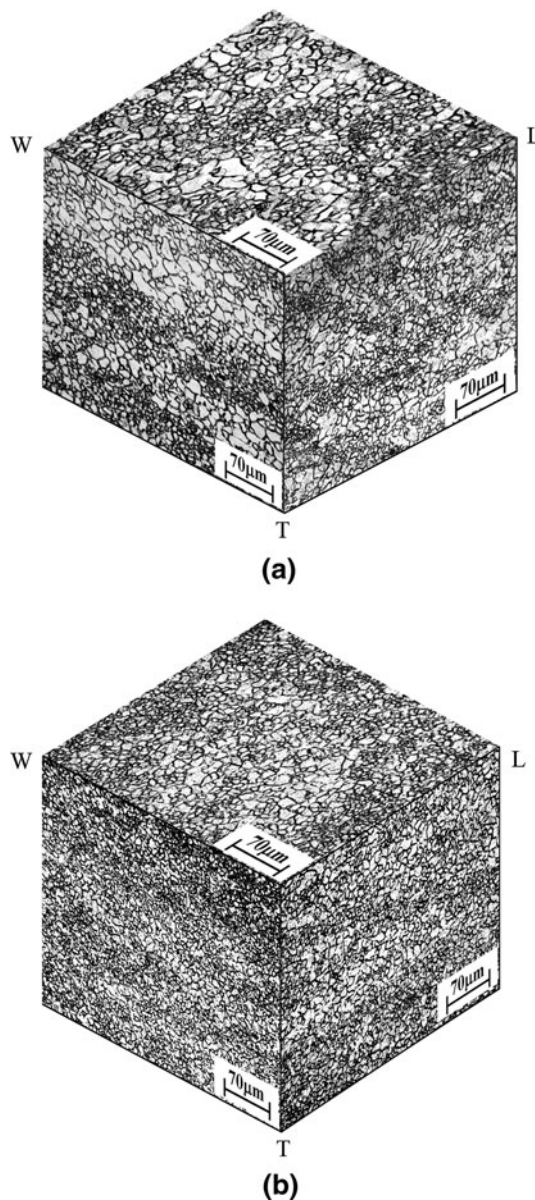


Fig. 2—BMs of two AZ31 alloys at three cross sections for (a) AZ31-SA and (b) AZ31-SB.

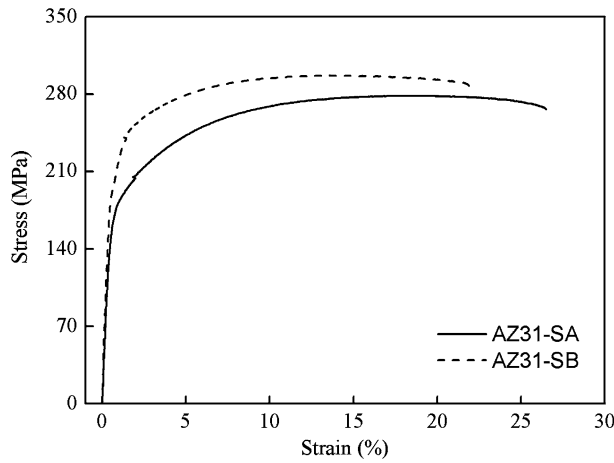


Fig. 3—Comparison of the tensile stress-strain curves of AZ31-SA and AZ31-SB base alloys.

Table III. A Comparison of Tension Test Data between AZ31-SA and AZ31-SB Alloys in the As-Received Condition

Alloy	Yield Stress MPa	UTS MPa	Elongation Pct
AZ31-SA	211	275	25
AZ31-SB	256	292	20

transverse (T) axis is perpendicular to the direction of width. Both alloys were observed to comprise equiaxed grains with an average grain size of $8.4 \mu\text{m}$ for AZ31-SA and $7.5 \mu\text{m}$ for AZ31-SB.

The tension-shear stress-strain curves for two kinds of AZ31 Mg alloy are shown in Figure 3. The AZ31-SA exhibited a lower yield stress and ultimate tension strength (UTS) but a higher strain-hardening rate and higher ductility than those of the AZ31-SB. All tension data of the as-received AZ31 alloys are listed in Table III. The AZ31-SA produced a yield stress of 211 MPa, UTS of 275 MPa, and elongation of 25 pct, whereas the yield stress of AZ31-SB was 256 MPa, UTS 292 MPa, and elongation 20 pct.

B. Mechanical Properties of Welds

Figure 4 shows the influence of welding current on nugget size. The nugget size increased with current. The size of AZ31-SB welds was obviously larger than that of AZ31-SA at the same current. This finding indicated that welds in AZ31-SB required lower heat inputs for formation than those in AZ31-SA. This result was not unexpected because AZ31-SB was thinner than AZ31-SA, leading to a lower liquid volume for any nugget size and a lower radial heat diffusion rate.^[24] Because the nugget size directly influences the strength of the weld, the relationship between tension-shear peak load and nugget size is drawn in Figure 5. It is shown that the peak load of both AZ31-SA and AZ31-SB increased exponentially with nugget size. Furthermore, it was noted that the peak load of AZ31-SA was larger than AZ31-SB at the same nugget size.

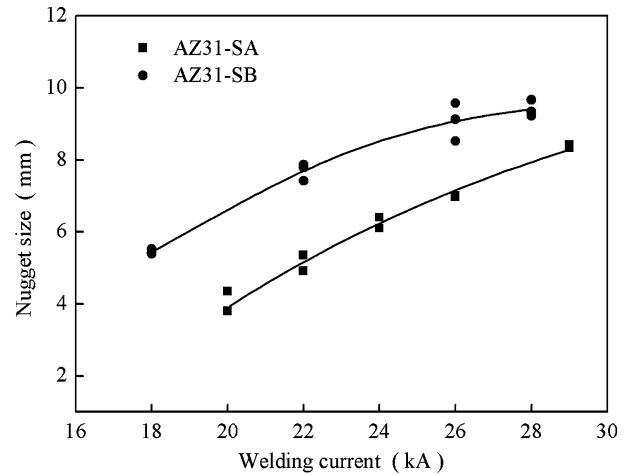


Fig. 4—Nugget size *vs* welding current.

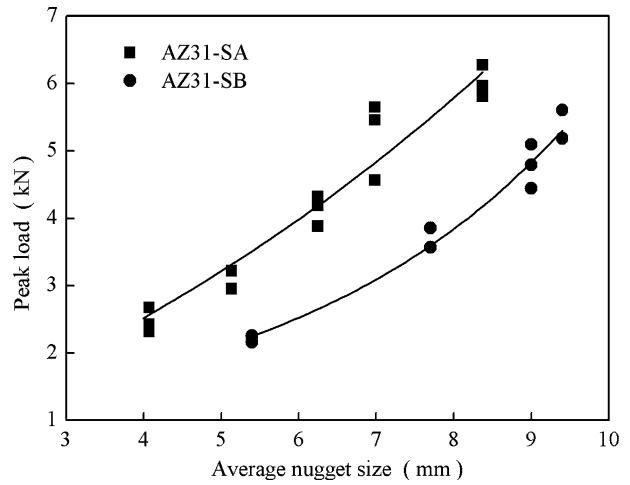


Fig. 5—Tension-shear load *vs* nugget size.

Sheet thickness can change the stress distribution and hence the joint strength even if they fail in an interfacial mode.^[25] This follows that because the sheet thickness of the two alloys is different, it is hard to state that the AZ31-SA joints are stronger than AZ31-SB joints simply based on Figure 5. As an alternative, Eq. [3] is used to normalize the effects of sheet thickness so that K_C can be plotted *vs* nugget size (Figure 6). As shown in Figure 6, the K_C increased with the increase of nugget size, which is a result of increasing welding current and will be discussed later in Section IV-D.

It is interesting to note in Figure 6 that the K_C of AZ31-SA joints is consistently higher than that of the AZ31-SB joints. This finding seems to conflict with the plane-stress–plane-strain transition model mentioned in the technical background section, which indicates a reduced K_C with an increased sheet thickness. But because Eq. [3] was derived for sheets with the same metallurgical properties, Figure 6 implies the AZ31-SA joints have an improved weld microstructure compared with AZ31-SB joints. In this connection, our previous study has showed that a favored CET in RSW fusion

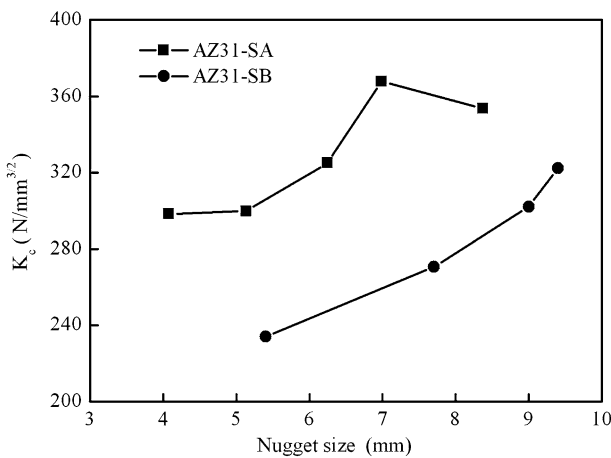


Fig. 6— K_c vs nugget size.

Table IV. Strength of Spot-Welded AZ31-SA (1.5 mm) and AZ31-SB (1.5 mm) Alloy

Alloy	Nugget Size mm	Peak Load kN	Nugget Size mm	Peak Load kN
AZ31-SA	4.8	2.6	7.6	4.0
AZ31-SB	5.4	2.2	7.7	3.7

zone in AZ31-SA alloy is because of micron-sized Al_8Mn_5 secondary particles only presented in the alloy compared with AZ31-SB alloy.^[18] To confirm this trend further, a few AZ31-SA samples were machined down to 1.5 mm in thickness and then spot welded with the same welding conditions to compare with AZ31-SB, as shown in Table IV. It is obvious that AZ31-SA joints outperformed AZ31-SB joints. But, because currently, it is not practical to have large quantity sheets with the same thickness, the rest of the work is conducted on the as-received sheet thickness (AZ31-SA in 2.0 mm and AZ31-SB in 1.5 mm). The weld microstructure will be examined in details in Section IV-C.

The stress distribution around the nugget is nonuniform,^[26] and the maximum stress occurs at the front face in line with the loading direction (point A and A' in Figure 1). This finding implies that fracture generally should initiate and propagate from those two regions. So the fracture morphology of the two areas could reflect the capacity for blocking crack propagation. Figure 7 compares the interfacial fracture surfaces of AZ31-SA and AZ31-SB around point A/A'. The fracture surface of AZ31-SB (Figure 7(b)) was relatively flatter and had less ductile tear traces than AZ31-SA (Figure 7(a)). This finding indicates that the energy absorbed in crack propagation in AZ31-SA was higher than that in AZ31-SB, which is consistent with the higher measured fracture toughness of AZ31-SA.

C. Effects of Microstructure

Microstructures near the notch should be related strongly to the toughness of the weld. Therefore, the typical morphology of solidification structures near the

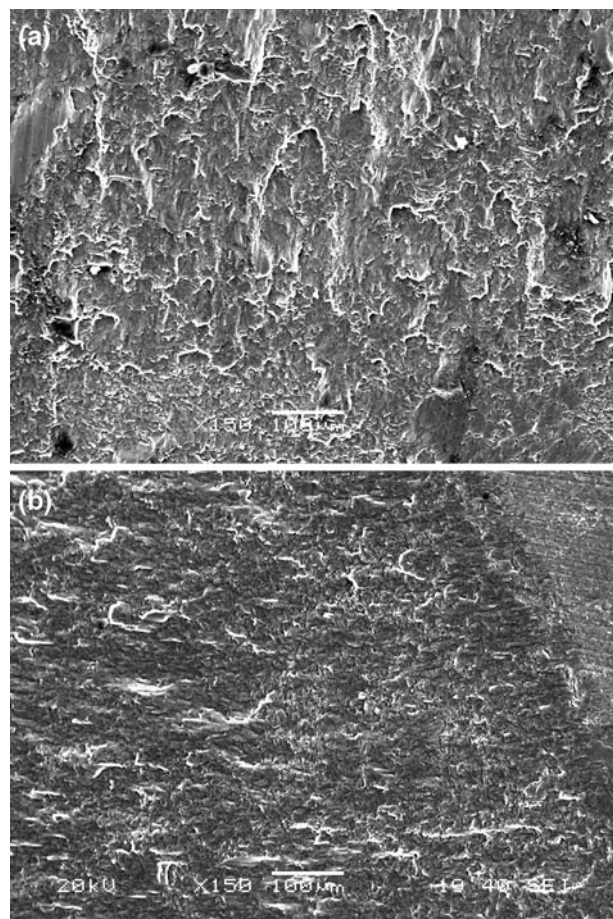


Fig. 7—SEM images of typical fracture morphology of interfacial failure in the periphery of fusion zone for (a) AZ31-SA, 24 kA and (b) AZ31-SB, 22 kA.

notch in RSW of AZ31-SA and AZ31-SB alloys is shown in Figures 8(a) and (b), respectively. Both alloys produced two zones with different microstructural features in the nugget (*i.e.*, columnar dendritic zone [CDZ] and equiaxed dendritic zone [EDZ]). The CDZ was adjacent to the fusion line and grew epitaxially from the solid–liquid boundary or the partially melted grains. The EDZ was located in the center of the nugget. The shape of the CET position was similar to that of the nugget.

It is interesting to note that the main difference between the two kinds of welds with 22 kA welding current and eight cycles welding time was favored CET in the AZ31-SA welds and also the morphology of CDZ. For AZ31-SA (Figure 8(a)), the homogeneous dendritic structure with short primary arms was formed along the fusion boundaries. In the fully penetrated weld, only a very narrow columnar dendritic structure existed along the fusion boundary. In most of the weld metal zone, equiaxed grains became the major solidification structure. However, typical columnar dendritic grains with long primary arms and a large columnar dendritic region were found in AZ31-SB (Figure 8(b)).

Equiaxed grain structures in castings and welds are usually more desirable than columnar structures for

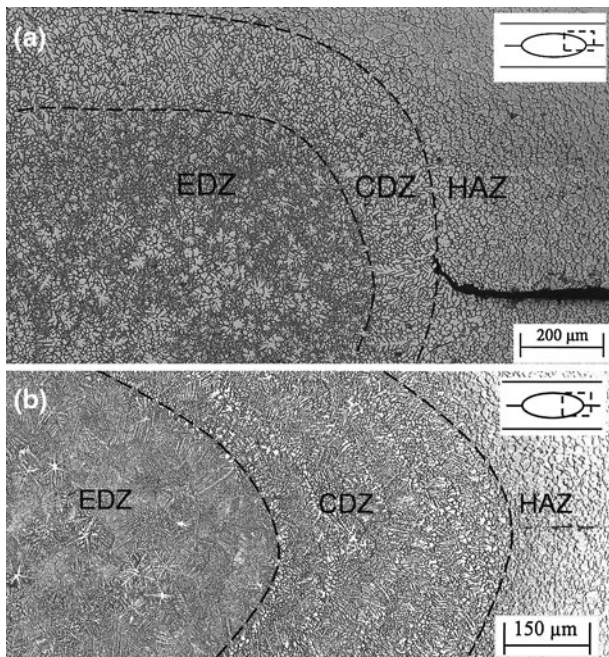


Fig. 8—Microstructures along the notch of the following AZ31 alloys: (a) AZ31-SA welded at 22 kA and (b) AZ31-SB welded at 22 kA.

several of the following reasons: the structures are more isotropic, equiaxed grains accommodate strains more uniformly, segregation of alloying elements to the central plane or region is reduced, and a smaller grain size enhances toughness.^[27] Zhang *et al.*^[16] reduced the formation of columnar structures in Al 6061 weldments by double arc welding, and consequently, metallurgical properties of welds were improved. Yongyuth *et al.*^[28] and Qiu *et al.*^[29] found that the toughness of castings and welds could be improved by increasing the volume fraction of the equiaxed zone. Furthermore, Yongyuth *et al.*^[28] observed that toughness changed with the specimen orientation. For example, the longitudinal transverse (LT) direction (the cracking plane coincided with the direction of growth of primary dendrites) produced the lowest toughness as a result of the anisotropy of dendrites. For spot welds, cracks propagated along the growth direction of primary dendrites, which is the weaker direction of fracture toughness as mentioned by Yongyuth *et al.*^[28] In addition, columnar dendritic structure can lead to the formation of a low melting point and brittle Mg₁₇Al₁₂ β -phase on dendritic boundaries because of microsegregation of Al along dendritic boundaries.^[30] It also could lead to the decrease of the toughness of AZ31-SB alloy welds with a large amount of columnar dendritic structure. Therefore, the improved CET in the AZ31-SA joints (with finer and shorter columnar dendrites) results in better mechanical properties.

Figure 9 shows the Vickers microhardness profiles of the RSW of AZ31-SA and AZ31-SB under the welding condition of 22 kA for eight cycles and 20 kA for eight cycles, respectively. For each alloy, the microhardness of the BM had the highest value (70 HV). Further analysis

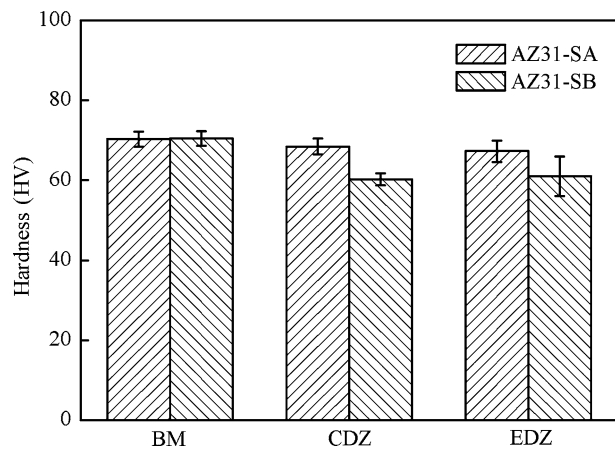


Fig. 9—Hardness profile across welds of two AZ31 alloys.

showed that the microhardness of each zone in the AZ31-SA weld was higher than that in AZ31-SB. The average microhardness of CDZ was about 69 HV in AZ31-SA and 60 HV in AZ31-SB, whereas the EDZ was 67 HV in AZ31-SA and 61 HV in AZ31-SB. The welding process resulted in the reduction of preexisting deformed structures such as solution strength, dislocation density, and defects in BM. Therefore, the weld produced a lower microhardness than BM. However, in the nugget, the AZ31-SA alloy produced finer grains than AZ31-SB. So the higher microhardness of the AZ31-SA weld compared with AZ31-SB is consistent with the Hall–Petch equation.

D. Effects of Welding Current

It was observed that for both AZ31-SA and AZ31-SB, the width of CDZ changed with the welding current. For AZ31-SA, the width of CDZ at the notch was about 146 μm when the welding current was 22 kA (Figure 8(a)). However, it reduced to near-zero when the current was greater than 24 kA (Figures 10(a) and (c)) and only was visible near the top and bottom of the nugget close to the electrode–workpiece interface (Figures 10(b) and (d)).

For AZ31-SB, the decrease of the width of CDZ close to the notch was more obvious, as shown in Figure 11. It was about 390 μm with a 22 kA welding current (Figure 8(b)), which was nearly three times that for AZ31-SA. When the welding current increased to 26 kA (Figure 11(a)), the CDZ at the notch was still visible but became shorter and finer. When the current was greater than 28 kA, the dendritic structure near the notch disappeared (Figure 11(b)). Like AZ31-SA, CDZ still could be found at the top and bottom of the nugget (Figure 11(c)). This finding could be because the water-cooled electrodes act as a large heat sink during cooling, which can lead to a high-temperature gradient along the electrode axis direction.

Considering the possible fluctuation of weld conditions and cross-section sample cutting positions, three samples per welding parameter were made for qualifying the different zones of microstructure. Figure 12 shows

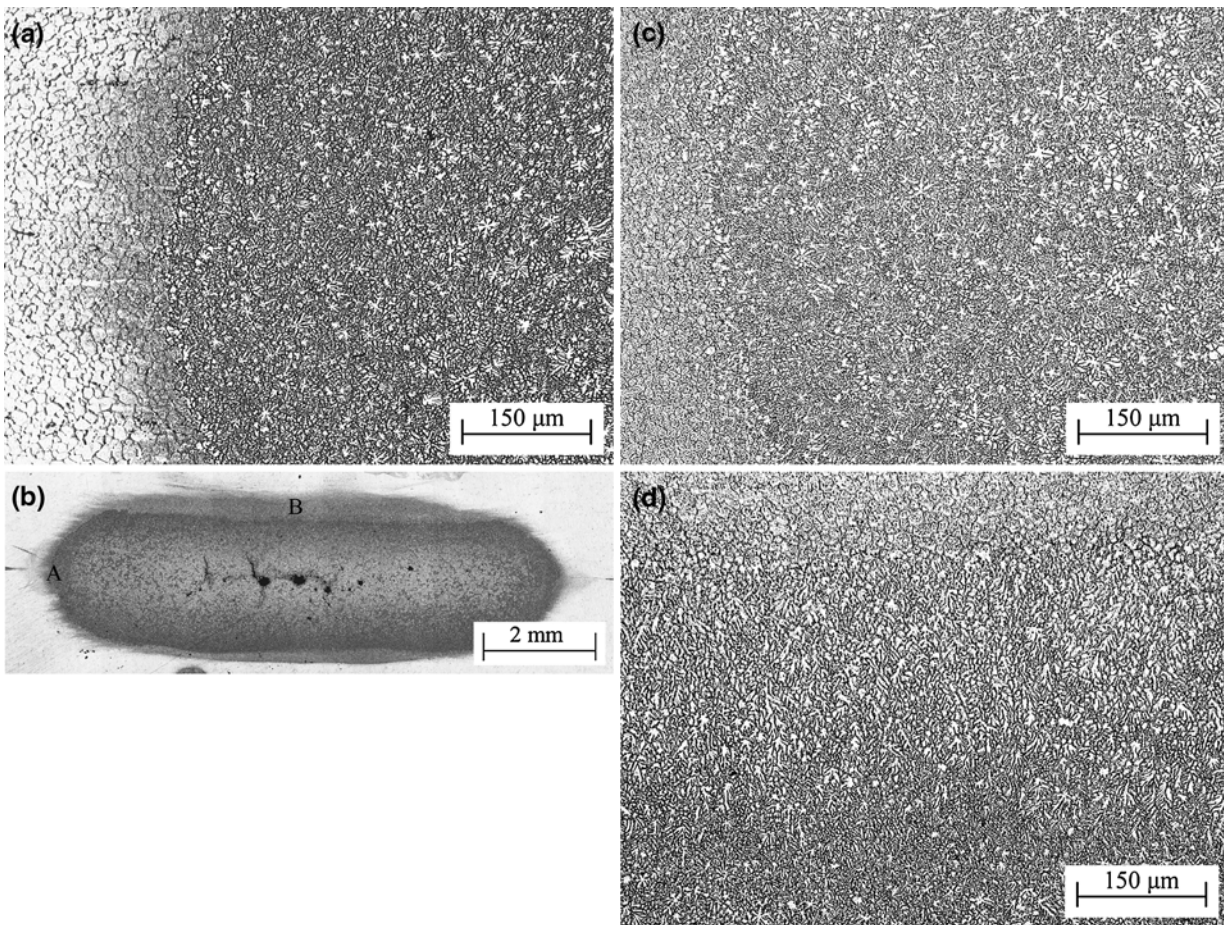


Fig. 10—Dendritic structure in AZ31-SA welds (a) at 24 kA and (b) at 28 kA. (c) The highlighted region A is the equiaxed structure near the notch, and (d) the highlighted region B is the dendritic structure at the top of the nugget.

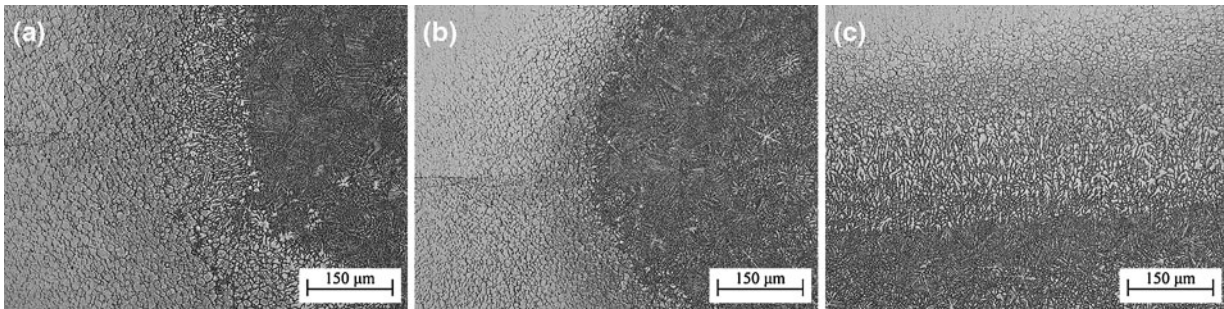


Fig. 11—Dendritic structure in AZ31-SB welds (a) at 26 kA near the notch, (b) at 28 kA near the notch, and (c) at 28 kA near to the electrode-workpiece interface.

the relationship between the width of CDZ close to the notch and the welding current. The CDZ width decreased linearly with the increase in welding current.

For a given alloy system, the morphology of the solidification structure is controlled by the ratio of G_L/R , where R is solidification growth rate and G_L is the thermal gradient in the liquid.^[31] A small G_L/R easily can produce an equiaxed dendritic structure, whereas a large G_L/R can produce a columnar dendritic structure.^[32] It is known that with the increase of heat input, the amount of penetration and melted metal increases.

This increase could induce a decrease of the thermal gradient during cooling.^[16] Consequently, the width of CDZ would decrease with the increase in welding current. According to the theory of Hunt, fully equiaxed growth occurs when the following is true^[32]:

$$G < 0.617 N_o^{1/3} \left\{ 1 - \frac{(\Delta T_N)^3}{(\Delta T_C)^3} \right\} \Delta T_C \quad [4]$$

where G is the maximum thermal gradient, N_o is the density of heterogeneous nucleants, ΔT_N is the critical

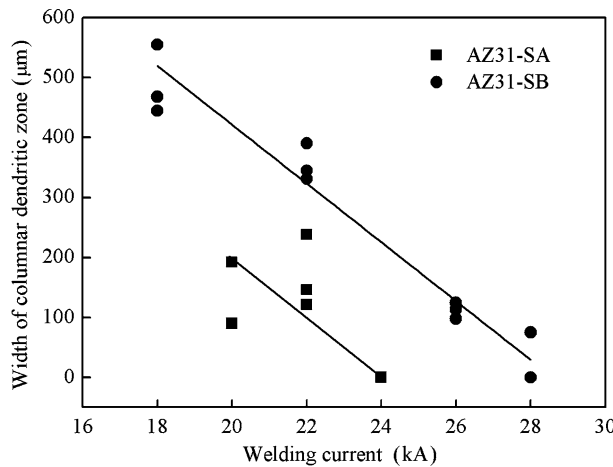


Fig. 12—Width of CDZ vs welding current.

undercooling for heterogeneous nucleation, and ΔT_C is the growth undercooling at the columnar front. It suggests that a supply of nucleation sites for new grains to develop and of thermal conditions for nucleation and grain growth are critical for equiaxed growth. Our previous study confirmed that the fraction of microscale Al_8Mn_5 particles was about 0.15 pct in the AZ31-SA alloy. It is hard to find microscale Al_8Mn_5 particles, and only nanoscale Al_8Mn_5 particles can be observed in AZ31-SB, which were not efficient for heterogeneous nucleation.^[18] Therefore, the critical G for CET should be lower in AZ31-SA than AZ31-SB. Then the current at which the CDZ disappeared at the nugget periphery of AZ31-SA would be lower than for AZ31-SB, as is observed.

So the change of mechanical properties should be related strongly to the change of CDZ. Similar to the tension-shear peak load (Figure 5), the K_C also increased with welding current, as shown in Figure 13. Combining Figures 12 and 13, Figure 14 shows the average CDZ width as a function of the average fracture toughness. It seems that the fracture toughness decreased linearly with the increase of CDZ width, suggesting the change in mechanical properties also should be related closely to the microstructure. Both alloys are fitted on the same curve, suggesting the correctness of the conclusion. Although the calculation of K_C contains various simplifying assumptions because of the boundary conditions of the theory (such as no plastic deformation, exactly round nugget, and simplification of analytic solutions), the inversely proportional relationship between K_C and the width of CDZ tends to confirm the negative effects of CDZ on the strength of these spot welds.

V. SUMMARY

RSW of two alloys, AZ31-SA and AZ31-SB, was performed in the present research. Only the interfacial failure mode was studied. Main conclusions are as follows:

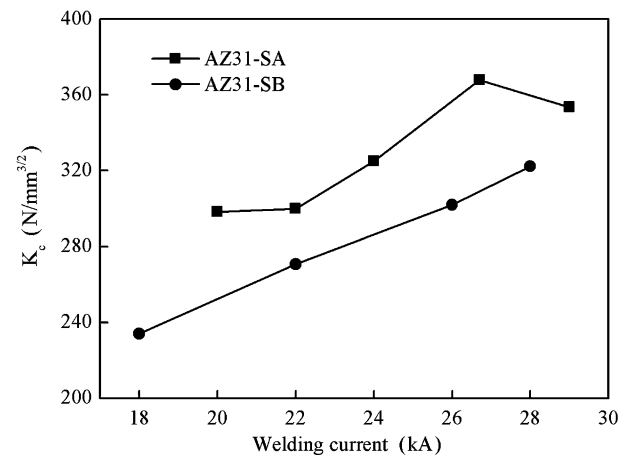


Fig. 13— K_C vs welding current.

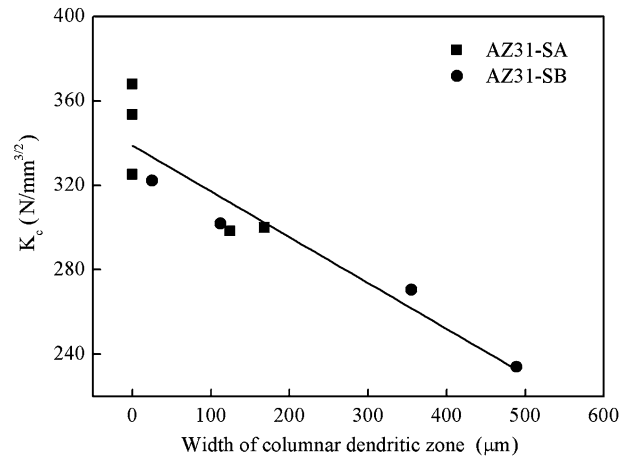


Fig. 14—Fracture toughness as a function of the width of CDZ.

1. For both welds of AZ31-SA and AZ31-SB, two zones can be divided from the fusion boundary into the nugget (*i.e.*, CDZ and EDZ). A short, fine, and narrow columnar dendrite area was found in AZ31-SA, whereas long primary arms, coarse grain size, and a well-developed columnar dendrite region was found in AZ31-SB. As a result, the fracture toughness of AZ31-SA welds is relatively higher because of this improved CET compared with AZ31-SB welds. This also is shown in the fracture surface of the AZ31-SA weld with more ductile tear traces and the relatively higher microhardness of AZ31-SA.
2. With the increase of welding current, the width of CDZ near the notch decreased linearly and became shorter and finer. CDZ width reached near-zero when the welding current was higher than a critical value, which was about 24 kA for AZ31-SA and 28 kA for AZ31-SB. For both AZ31-SA and AZ31-SB welds, the inversely proportional relationship between K_C and the width of CDZ suggests that columnar dendritic structure has an adverse effect on the fracture toughness of a magnesium alloy.

ACKNOWLEDGMENTS

This research was supported financially by the Natural Sciences and Engineering Research Council (NSERC) of Canada, AUTO21 Network Centres of Excellence of Canada, and NSERC Magnesium Network (MagNET). The authors want to thank Professors. S. Lawson, G.S. Zou and L.Q. Li for their suggestions in this work.

REFERENCES

1. L.M. Liu, G. Song, and M.L. Zhu: *Metall. Mater. Trans. A*, 2008, vol. 39A, pp. 1702–11.
2. C.T. Chi and C.G. Chao: *J. Mater. Process. Tech.*, 2007, vol. 182, pp. 369–73.
3. L.M. Liu, H.Y. Wang, and Z.D. Zhang: *Scripta Mater.*, 2007, vol. 56, pp. 473–76.
4. M. Yamamoto, A. Gerlich, T.H. North, and K. Shinozaki: *J. Mater. Sci.*, 2007, vol. 42, pp. 7657–66.
5. Y.R. Wang, Z.H. Mo, J.C. Feng, and Z.D. Zhang: *Sci. Technol. Weld. Join.*, 2007, vol. 12, pp. 671–76.
6. L. Liu, S.Q. Zhou, Y.H. Tian, J.C. Feng, J.P. Jung, and Y. Zhou: *Sci. Technol. Weld. Join.*, 2009, vol. 14, pp. 356–61.
7. D.Q. Sun, B. Lang, D.X. Sun, and J.B. Li: *Mater. Sci. Eng. A*, 2007, vols. 460–1, pp. 494–98.
8. S. Kou: *Welding Metallurgy*, Wiley, New York, NY, 2002, p. 188.
9. A.F. Norman, K. Hyde, F. Costello, S. Thompson, S. Birley, and P.B. Prangnell: *Mater. Sci. Eng. A*, 2003, vol. 354, pp. 188–98.
10. M.H. Burden and J.D. Hunt: *Metall. Trans. A*, 1975, vol. 6, pp. 240–41.
11. V.B. Biscuola and M.A. Martorano: *Metall. Mater. Trans. A*, 2008, vol. 39A, pp. 2885–95.
12. A.E. Ares and C.E. Schvezov: *Metall. Mater. Trans. A*, 2000, vol. 31A, pp. 1611–25.
13. B.P. Pearce and H.W. Kerr: *Metall. Trans. B*, 1981, vol. 12B, pp. 479–86.
14. W.L. Dai: *Mater. Lett.*, 2003, vol. 57, pp. 2447–54.
15. L. He, M. Wu, L. Li, and H. Hao: *Appl. Phys. Lett.*, 2006, vol. 89, p. 131504.
16. Y.M. Zhang, C. Pan, and A.T. Male: *Metall. Mater. Trans. A*, 2000, vol. 31A, pp. 2537–43.
17. S. Kou and Y. Le: *Metall. Trans. A*, 1988, vol. 19A, pp. 1075–82.
18. L. Xiao, L. Liu, Y. Zhou, and S. Esmaeli: *Metall. Mater. Trans. A*, 2010, vol. 41A, pp. 1511–22.
19. S. Zhang: *Inter. J. Fracture*, 1997, vol. 88, pp. 167–85.
20. S. Zhang: *Weld. J.*, 2001, vol. 80 (8), pp. 201s–3s.
21. S.I. Rokhlin and L. Adler: *J. Appl. Phys.*, 1984, vol. 56 (3), pp. 726–31.
22. T.L. Anderson: *Fracture Mechanics: Fundamentals and Applications*, CRC Press, Boca Raton, FL, 1995, pp. 87–89.
23. Y.J. Chao: *Sci. Technol. Weld. Join.*, 2003, vol. 8 (2), pp. 133–37.
24. M. Marya and X.Q. Gayden: *Weld. J.*, 2005, vol. 84, pp. 172s–82s.
25. D. Radaj and S. Zhang: *Eng. Fract. Mech.*, 1991, vol. 39, pp. 391–13.
26. Y.J. Chao: *J. Eng. Mater. Technol.*, 2003, vol. 125 (2), pp. 125–32.
27. J.C. Villafuerte, H.W. Kerr, and S.A. David: *Mater. Sci. Eng. A*, 1995, vol. 194, pp. 187–91.
28. P. Yongyuth, P.K. Ghosh, P.C. Gupta, A.K. Patwardhan, and S. Prakash: *ISIJ Int.*, 1992, vol. 32, pp. 771–78.
29. Y. Qiu, G. Jia, X. Liu, and G. Wang: *J. Iron Steel Res. Int.*, 2006, vol. 13, pp. 67–69.
30. S. Kleiner, O. Beffort, A. Wahlen, and P.J. Uggowitzer: *J. Light Metal.*, 2002, vol. 2, pp. 277–80.
31. S. Kou: *Welding Metallurgy*, Wiley, New York, NY, 1987, p. 211.
32. J.D. Hunt: *Mater. Sci. Eng. A*, 1984, vol. 65, pp. 75–83.